

# Fermi surfaces and Phase Stability of $\text{Ba}(\text{Fe}_{1-x}\text{M}_x)_2\text{As}_2$ ( $M=\text{Co}, \text{Ni}, \text{Cu}, \text{Zn}$ )

S. N. Khan,<sup>1,2</sup> Aftab Alam,<sup>3</sup> and Duane D. Johnson<sup>1,2,4\*</sup>

<sup>1</sup>*Department of Physics, University of Illinois, Urbana-Champaign, Illinois 61801, USA;*

<sup>2</sup>*The Ames Laboratory, US Department of Energy, Ames, Iowa 50011-3020, USA;*

<sup>3</sup>*Department of Physics, Indian Institute of Technology, Bombay, Powai, Mumbai 400 076, India and*

<sup>4</sup>*Department of Materials Science & Engineering, Iowa State University, Ames, Iowa 50011-2300.*

(Dated: May 17, 2022)

$\text{BaFe}_2\text{As}_2$  with transition-metal doping exhibits a variety of rich phenomenon from coupling of structure, magnetism, and superconductivity. Using density functional theory, we systematically compare the Fermi surfaces (FS), formation energies ( $\Delta E_f$ ), and density of states (DOS) of electron-doped  $\text{Ba}(\text{Fe}_{1-x}\text{M}_x)_2\text{As}_2$  with  $M=\{\text{Co}, \text{Ni}, \text{Cu}, \text{Zn}\}$  in tetragonal ( $I4/mmm$ ) and orthorhombic ( $Fmmm$ ) structures in nonmagnetic (NM), antiferromagnetic (AFM), and paramagnetic (PM, disordered local moment) states. We explain changes to phase stability ( $\Delta E_f$ ) and Fermi surfaces (and nesting) due to chemical and magnetic disorder, and compare to observed/assessed properties and contrast alloy theory with that expected from rigid-band model. With alloying, the DOS changes from common-band (Co,Ni) to split-band (Cu,Zn), which dictates  $\Delta E_f$  and can overwhelm FS-nesting instabilities, as for Cu,Zn cases.

PACS numbers: 71.15.Nc, 71.18.+y, 74.20.Pq, 74.70.Xa

## I. INTRODUCTION

The Fe-based superconductors (Fe-SCs) are providing new avenues to explore high- $T_c$  superconductivity (SC) involving magnetism.<sup>1-6</sup>  $\text{BaFe}_2\text{As}_2$  (BFA) has been of particular interest due to its ease of synthesis. The parent compound exhibits AFM order at a Néel temperature of  $T_N = 140$  K and this order is suppressed in favor of SC on chemical doping.<sup>7-10</sup> Electron doping can be achieved by substituting a transition metal for Fe to give a metal-substituted solid solution M-BFA,<sup>9,10</sup> with an increasing electron-per-Fe ( $e/\text{Fe}$ ) count. Notably, different behaviors for chemical and magnetic ordering instabilities are found for Co,Ni versus Cu,Zn solid-solutions, for example, with (in)commensurate AFM order depending on the dopant, with possible coexistence of SC and AFM order. Interestingly, Cr-based binary, metallic alloys<sup>11,12</sup> show the same coexistence behavior but with  $T_c$  an order of magnitude smaller than Fe-SCs. Although numerous experimental studies on electron-doped BFA have been carried out over the last few years, a systematic theoretical investigation is still lacking. Here, we address  $\text{Ba}(\text{Fe}_{1-x}\text{M}_x)_2\text{As}_2$  via a proper alloy theory to provide a direct comparison of trends and explain their origin.

To provide a single theoretical description within density functional theory (DFT), we use KKR multiple-scattering theory combined with the coherent-potential approximation (CPA)<sup>13</sup> to handle chemical and magnetic disorder. For M-BFA in high- $T$   $I4/mmm$  and low- $T$   $Fmmm$  structures<sup>14</sup> with increasing  $e/\text{Fe}$  in the NM, PM, and AFM states, the KKR-CPA is used to examine relative phase stability ( $\Delta E_f$ ), Fermi surface topologies and nesting (electron-hole) features through the Bloch spectral functions,<sup>15</sup> and changes of the density of states (DOS) due to alloying and disorder, as well as to contrast these results to expectations from a rigid-band model.

## II. BACKGROUND

Generally, DFT results on BFA match the striped AFM ordering<sup>16</sup> and measured electronic structure quite well. The FS exhibits two or three hole cylinders at the zone center ( $\Gamma$ ) and two electron cylinders at the zone corner ( $X$ ), as observed in DFT<sup>17</sup> and angle-resolved photoemission<sup>18-20</sup> (ARPES). The prominent  $(\pi,\pi)$  FS nesting between these cylinders helps stabilize the AFM state,<sup>2</sup> and spin fluctuations in this mode may drive Cooper pairing.<sup>21,22</sup> Hence, the need to study FS nesting and disorder broadening effects.

The M-BFA phase diagrams show suppressed AFM ordering in favor of a neighboring SC state. The SC domes have M-fraction  $x=0.03-0.12$ ,  $0.02-0.08$ , and  $\sim 0.04$  with  $T_c^{max}$  of 23, 20, and 2 K for Co-, Ni-, and Cu-BFA, respectively.<sup>8,9</sup> Zn-doped samples do not superconduct. Notably,  $T_c^{max}$  occurs near the extrapolated AFM quench concentration.<sup>8,9</sup> For Co- and Ni-BFA, the magnetic order becomes an incommensurate spin-density wave before entering the SC state, which emphasizes itinerancy and import of FS nesting.<sup>23</sup> Cu-BFA remains commensurate.<sup>23</sup> And, no changes in the magnetism or FS are found in Zn-BFA.<sup>24</sup> In addition, there are steric effects due to changing  $a$  and  $c$  lattice constants in  $I4/mmm$  structure.  $a$  is almost unchanged for Co-BFA and increases for Ni-, Cu-, and Zn-BFA. For Co-, Ni-, Cu-BFA  $c$  shrinks<sup>25-27</sup> and for Zn-BFA it increases.<sup>28</sup>

Lastly, there is debate on whether M-BFA follows a rigid-band picture; and, if not, whether an effective Fermi level shift is still applicable. In a rigid-band model, the electronic structure is fixed to that of  $\text{BaFe}_2\text{As}_2$  and the Fermi energy is raised by the amount of additional  $e/\text{Fe}$  for each dopant: Co (1e), Ni (2e), Cu (3e), and Zn (4e). The atomic species of the dopant becomes irrelevant (even though the atomic number  $Z_i$  increases and

changes the scattering properties relative to Fe), and all dopants should generate the same electronic effects for a given  $e/\text{Fe}$ , the validity of which alloy theory can make clear assessments. While ARPES shows similar trends with nominal  $e/\text{Fe}$  for Co- and Ni-BFA, there are deviations from rigid-band for Cu- and Zn-BFA.<sup>24,29</sup> By Luttinger's theorem<sup>30</sup>, an effective  $e/\text{Fe}$  can be defined from changes in the experimentally measured FS. The phase diagrams of Co-, Ni-, and Cu-BFA have been found to approximately coincide in this manner.<sup>29</sup> Zn-BFA shows no measurable changes in FS and no superconductivity.<sup>24</sup> Comparing supercell calculations for Co- and Zn-BFA show that Co-BFA obeys rigid-band while Zn-BFA does not.<sup>31</sup> The rigid-band model is applicable as long as site-potential differences between Fe and dopant are much less than bandwidths. As we show, these differences are visible in a dopant's site-projected DOS, where significant overlap between Fe  $d$ -states and those of Co or Ni exists, less so for Cu, and almost none for Zn.<sup>32</sup> We find that the FS evolves similar to that expected from rigid-band for Co-, Ni-, and Cu-BFA but not for Zn-BFA; yet, deviations from rigid-band behavior are readily apparent in  $\Delta E_f$  for PM Cu-BFA.

### III. COMPUTATIONAL DETAILS

DFT calculations at 0 K were performed using an all-electron, KKR-CPA Green's function method.<sup>13,33,34</sup> To improve the usual site-centered basis set, empty spheres (E1, E2, and E3) were inserted at interstitial voids in the structure (Table I). The local density approximation (LDA) to DFT is used and the coherent potential approximation (CPA) is used to address both chemical and magnetic disorder.<sup>35</sup> For the PM state, uncorrelated, randomly-oriented local moments are described by an approximate disordered local moment (DLM) state,<sup>36</sup> where such localized magnetic disorder can produce large energy broadening of the electronic states, which is reduced with magnetic short-range order included (beyond the CPA<sup>37</sup>), but changes FS nesting contributions to the magnetic susceptibility.<sup>38</sup> Often, the DLM state (site magnetizations  $m_i \neq 0$ ) is a more appropriate representation of the PM state than the NM state ( $m_i = 0$ ) typically assumed in theory for comparison to experiment,<sup>39,40</sup> such as for magnetic transition temperatures in magnetic metals.<sup>35,41</sup>

All results were obtained with a  $8 \times 8 \times 8$  Monkhorst-Pack  $k$ -point mesh for Brillouin zone (BZ) integrals,<sup>42</sup> and using complex energy ( $E$ ) contour integration with 25  $E$ -points on a Gauss-Legendre semi-circular contour.<sup>43</sup> Fermi energies were determined from an analytic, integrated DOS (Lloyd's) formula<sup>44</sup> to yield an accurate electron count. The valence configurations were taken as Ba  $5p^6 6s^2$ , Fe  $4s^2 3d^6$ , Co  $4s^2 3d^7$ , Ni  $4s^2 3d^8$ , Cu  $4s^2 3d^9$ , Zn  $4s^2 3d^{10}$ , and As  $4s^2 4p^3$ . To match the  $e$ -per-volume of the  $\text{BaFe}_2\text{As}_2$  samples probed in experiment, the

TABLE I. Atomic coordinates and sphere sizes for atoms and empty spheres (E1-3).  $I4/mmm$  ( $Fmmm$ ) has body-centered tetragonal (face-centered orthorhombic) unit vectors.

Site	Coordinates	Wyckoff	Radius ( $pm$ )
<i>I4/mmm</i>			
Ba	(0.0000 <i>a</i> , 0.0000 <i>a</i> , 0.0000 <i>c</i> )	2a	225.1
Fe(M)	(0.5000 <i>a</i> , 0.0000 <i>a</i> , 0.0000 <i>c</i> )	4d	136.5
As	(0.0000 <i>a</i> , 0.0000 <i>a</i> , 0.3545 <i>c</i> )	4e	136.5
E1	(0.5000 <i>a</i> , 0.5000 <i>a</i> , 0.0000 <i>c</i> )	2b	76.3
E2	(0.0000 <i>a</i> , 0.0000 <i>a</i> , 0.2072 <i>c</i> )	4e	78.9
E3	(0.2007 <i>a</i> , 0.2007 <i>a</i> , 0.1715 <i>c</i> )	16m	55.8
<i>Fmmm</i>			
Ba	(0.0000 <i>a</i> , 0.0000 <i>b</i> , 0.0000 <i>c</i> )	4a	224.4
Fe(M)	(0.2500 <i>a</i> , 0.2500 <i>b</i> , 0.2500 <i>c</i> )	8f	136.1
As	(0.0000 <i>a</i> , 0.0000 <i>b</i> , 0.3545 <i>c</i> )	8i	136.1
E1	(0.5000 <i>a</i> , 0.0000 <i>b</i> , 0.0000 <i>c</i> )	4b	76.1
E2	(0.0000 <i>a</i> , 0.0000 <i>b</i> , 0.2072 <i>c</i> )	8i	78.6
E3	(0.2007 <i>a</i> , 0.0000 <i>b</i> , 0.1715 <i>c</i> )	16n	55.7

lattice constants (in  $pm$ ) were fixed to experiment:<sup>14</sup>  $a = b = 396.25$  and  $c = 1301.68$  for the  $I4/mmm$  structure, and  $a = 561.46$ ,  $b = 557.42$ , and  $c = 1294.53$  for the  $Fmmm$  structure. As the alloy concentrations are sufficiently low, we fixed the lattice to minimize DFT (relative) error and isolate electronic and steric effects.

Fermi surfaces were determined at  $E_F$  via the Bloch spectral function  $A(\mathbf{k}, E) = -\frac{1}{\pi} \text{Im} G(\mathbf{k}, E)$ , where  $G$  is the single-particle Green's function.  $A(\mathbf{k}, E)$  is the  $E$ - and  $\mathbf{k}$ -space resolved DOS and dispersion. In the limit of an ordered compound it reduces to Dirac  $\delta$ -functions that define the band structure  $E(\mathbf{k})$ . In the presence of magnetic or chemical disorder there is  $\mathbf{k}$ -dependent spectral broadening and shifting due to impurity scattering handled via the CPA. The spectral full-width at half-maximum with respect to energy is inversely proportional to the lifetime of electronic states,<sup>45,46</sup> which also dictate transport and SC properties. Spectral broadening also can support coexistence of AFM and SC, as found, for example, in binary Cr alloys, such as Cr-Ru.<sup>11</sup>

## IV. RESULTS

### A. Phase Stability with Alloying

For an alloy with lattice parameters ( $a, b, c$ ), the formation energies is defined, relative to the concentration-weighted sum of the energy of the (Ba, Fe, M, As) constituents in their respective equilibrium structures. However, in a fixed host,  $\Delta E_f$  trends for  $\text{Ba}(\text{Fe}_{1-x}\text{M}_x)_2\text{As}_2$  versus  $x$  (or  $e/\text{Fe}$ ) are more simply revealed referencing

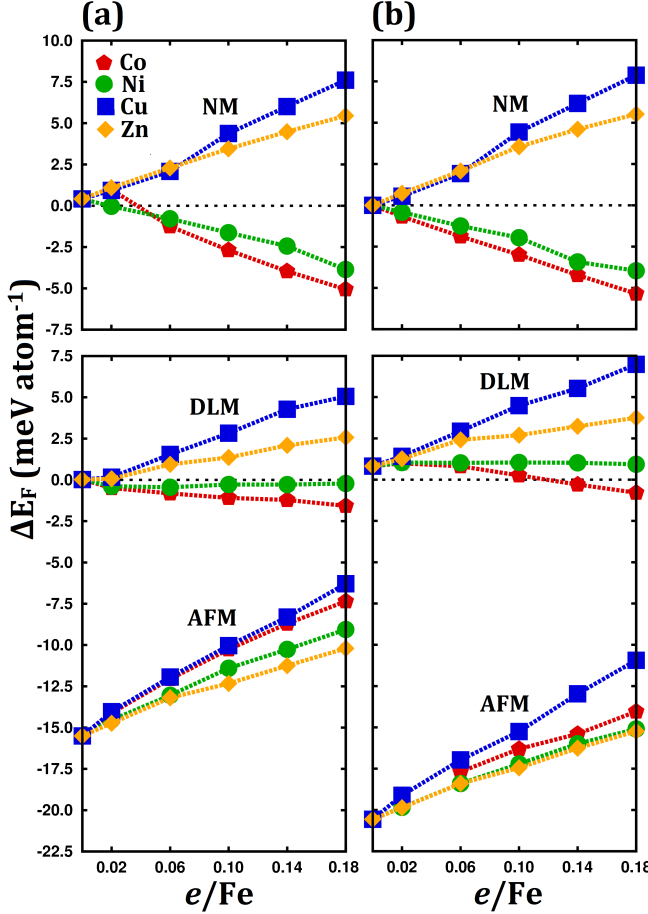


FIG. 1. (Color online) Formation energy of NM, DLM, and AFM  $\text{Ba}(\text{Fe}_{1-x}\text{M}_x)_2\text{As}_2$  relative to mixed phase NM endpoints  $\text{BaFe}_2\text{As}_2$  and  $\text{BaM}_2\text{As}_2$  in (a)  $I4/mmm$  and (b)  $Fmmm$  structural phases. Nominal  $e/\text{Fe}$  counting is used.

$\text{BaFe}_2\text{As}_2$  and  $\text{BaM}_2\text{As}_2$ , i.e.,

$$\Delta E_f = E^{\text{Ba}(\text{Fe}_{1-x}\text{M}_x)_2\text{As}_2} - [(1-x)E^{\text{BaFe}_2\text{As}_2} + xE^{\text{BaM}_2\text{As}_2}]. \quad (1)$$

Figure 1 shows  $\Delta E_f$  of the NM, DLM, and AFM states versus nominal  $e/\text{Fe}$  for each M, plotted relative to the mixed phase with NM  $\text{BaFe}_2\text{As}_2$  and  $\text{MFe}_2\text{As}_2$ .

At zero doping, the NM and DLM energies are nearly degenerate. At finite temperatures the DLM state will have a lower free-energy because of the spin-disorder entropy. The AFM state is 16 ( $I4/mmm$ ) or 21 meV/atom ( $Fmmm$ ) below the NM state. In experiments on BFA, the magnetic and structural phase transition occur simultaneously in BFA at 140 K (or 12 meV).<sup>8</sup> Previous DFT studies find 37 meV/atom ( $I4/mmm$ ) using full-potential augmented plane waves (FLAPW)<sup>17</sup> or 70 meV/atom ( $Fmmm$ ) using pseudopotentials,<sup>16</sup> which is the available data.

For magnetism, we find Fe site moments ( $I4/mmm$ ) are 1.4  $\mu_B$  (AFM) and 1.0  $\mu_B$  (DLM). For  $Fmmm$ , there

is only a slight drop to 1.3  $\mu_B$  (AFM) and 0.95  $\mu_B$  (DLM). We do not find symmetry breaking to lead to a significant change of site moments. As a contrast, we note local, Heisenberg models, often fit to spin-wave spectra, find very different  $J_{1a}$  and  $J_{1b}$  nearest neighbor exchange parameters with broken symmetry.<sup>47,48</sup> We see, however, that magnetic disorder leads to a large reduction in site moments, due to transverse components of the magnetization. The time-averaged ordered moment is 0.9  $\mu_B$  from neutron diffraction,<sup>49</sup> which have some transverse components. Using core-electron spectroscopy to probe short-time scales ( $10^{-15}$  sec), the measured moment is 2.1  $\mu_B$  in the closely related  $\text{SrFe}_2\text{As}_2$ .<sup>39</sup> This difference has been attributed to modest electron correlations<sup>40</sup> and magnetic excitations.<sup>50</sup> We see here that the disordered component of the site moment is substantial. Overall, the KKR results agree reasonably with previously computed AFM site moments of 1.8  $\mu_B$  ( $I4/mmm$ ) from FLAPW; the moments are 2.6  $\mu_B$  ( $Fmmm$ ) using pseudopotentials.

In this low-doping regime ( $e/\text{Fe} \leq 0.18$ ), the  $\Delta E_f$  vary linearly with  $x$  or  $e/\text{Fe}$  for all magnetic states and structures. Furthermore, the resulting trends are robust whether considering the  $I4/mmm$  or  $Fmmm$  structures. In the NM state, there is a clear splitting in the behavior of Co- and Ni-BFA versus Cu- and Zn-BFA. Both Co- and Ni-BFA show the same, favorable formation energies for given  $e/\text{Fe}$ . Cu- and Zn-BFA also agree for given  $e/\text{Fe}$  but are unfavorable to mixing at zero temperature. Chemical mixing entropy does reduce formation enthalpies relative to endpoints  $\text{BaFe}_2\text{As}_2$  and  $\text{BaM}_2\text{As}_2$ , increasing the favorability of the higher  $e/\text{Fe}$  compounds. In an ideal mixing model<sup>51</sup> this will reduce the free energy by 21, 13, 10, and 8 meV/atom for Co-, Ni, Cu-, and Zn-BFA at  $e/\text{Fe} = 0.18$  and 1000 °C, a typical annealing temperature.<sup>8,9</sup> This effect is not accounted for in the 0 K results in Fig. 1 so as to separate electronic ( $e/\text{Fe}$ ) effects from entropic (dopant  $x$ ) effects.

In the DLM state, a similar splitting persists, but energies are less pronounced. There is also less agreement in the energies of Cu- and Zn-BFA at a given  $e/\text{Fe}$ . We find no magnetic moments at the dopant atom and only marginally reducing moments on the Fe sites with increasing  $e/\text{Fe}$ . Neutron diffraction shows a rapid drop in Fe moment with doping.<sup>23</sup> This may be a result of the sensitivity of the moment to an increasing  $a$  lattice constant.<sup>52</sup> Experiments that demonstrate the incommensurability of the spin-density wave<sup>23</sup> on Co and Ni doping are done in the PM state. Cu-BFA does not become incommensurate. Our results show Cu mixing is, at best, weakly favorable. Thus, the lack of incommensurate splitting in Cu might arise not as a result of a FS effects, but rather due Cu clustering. In the AFM state, dopants decrease favorability relative to the PM state. This is in qualitative agreement with the known phase diagrams, where dopants suppress the AFM state and eventually lead to SC. The dopant species splitting

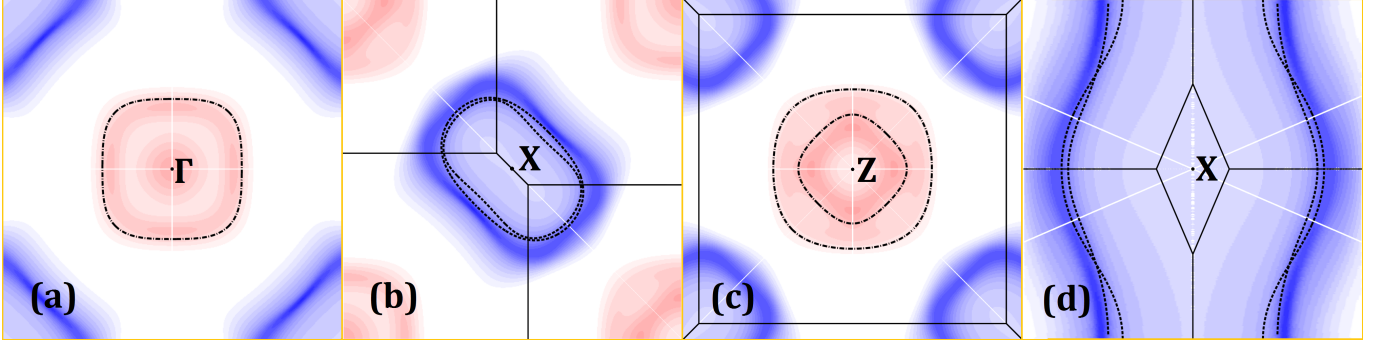


FIG. 2. (Color online) Bloch spectral function  $A(\mathbf{k}, E)$  of  $\text{BaFe}_2\text{As}_2$  in both NM and DLM states. Hole cylinders are depicted as dash-dot lines (NM) or false-color scaled red (DLM). Electron cylinders are dashed (NM) or blue (DLM). Solid lines indicate the BZ boundary. Cross-sections are normal to (a) [001] about  $\Gamma$ , (b) [001] about X, (c) [001] about Z, and (d)  $[\bar{1}10]$  about X. False coloring is mapped (in  $10^3$  states  $\text{Ryd}^{-1}\text{cell}^{-1}$  r.u. $^{-3}$ ) as  $\{0 \leftrightarrow \text{RGB } 0\text{xFFFFFF (white)}, 100 \leftrightarrow \text{RGB } 0\text{x770000 (light red)}, \text{ and } 1000 \leftrightarrow \text{RGB } 0\text{xFF0000 (red)}\}$  for hole pockets. And similarly for electron pockets. This choice was made to make as many features as possible visible across plots.

here is even less pronounced and all compounds follow nearly the same trend with  $e/\text{Fe}$ . This suggests an important difference in doping effects on the PM and AFM state. Note that prior DFT calculations for the doped compounds have been performed on the NM state.<sup>31,32</sup>

### B. Fermi Surfaces of PM States

Figure 2 shows the FS of NM and DLM  $\text{BaFe}_2\text{As}_2$ . NM surfaces are shown for electrons (dashed lines) or holes (dash-dot lines) – there is no FS broadening with no chemical disorder – and these surfaces agree with previous results. The Brillouin zone (solid lines) and labels correspond to the body-centered tetragonal lattice and can be found in the literature.<sup>53</sup> DLM surfaces for electrons (blue) or holes (red) show significant broadening due to local orientational disorder – in contrast to chemical disorder, which we see, below, is less significant. The approximate  $\mathbf{k}$ -space broadening is  $0.14$  r.u. (reciprocal units defined as  $2\pi/a$  units in  $\mathbf{k}$ -space).

Note that DLM Bloch spectral peaks do not coincide exactly with the NM surface. The DLM hole (electron) pockets are reduced (enlarged) in size relative to the NM. This corresponds to an effective  $e$ -doping, as reflected in the DOS with a positive shift of  $E_F$ . The interior pocket near the Z point is pinched off near the  $\Gamma$  point. This can vary with choice of code and lattice parameters. A strong pinching is also visible in prior DFT calculations<sup>17</sup> and ARPES<sup>20,29</sup>. The outer cylinder is fairly uniform and gives rise to strong nesting with electron cylinders. The electron cylinders obey a  $4_1$  screw symmetry along the  $k_z$ -axis while the hole cylinders obey  $90^\circ$  rotational symmetry. The DLM broadening and  $E_F$  shift changes the strength of nesting between hole and electron cylinders. The large broadening can explain the reduced resolution of ARPES data, especially when compared to measure-

ments made on CuO SCs.

To make a connection to nesting, we note that it is, in principle, possible to calculate the chemical, magnetic and magneto-chemical susceptibilities within the KKR-CPA using a thermodynamic linear-response theory,<sup>54</sup> similar to phonon linear-response that uses infinitesimal displacements. For such susceptibilities in the high-symmetry (chemically or magnetically disordered) state, the correct functional form is  $\chi^{-1}(\mathbf{q}; T) = [1 - \beta(1 - m_i^2)S^{(2)}(\mathbf{q}, T)]$ , where  $\beta = (k_B T)^{-1}$  and  $S^{(2)}(\mathbf{q}, T)$  is an exact second-variation of the electronic grand-potential with respect to fluctuations, e.g., site magnetization, and historically initiated by Orstein and Zernike. For an Ising-like system,  $S^{(2)}(\mathbf{q}, T)$  plays the role of a thermodynamically averaged pairwise  $J(\mathbf{q})$ . Such calculations have been done for solid-solutions<sup>54–57</sup> and elemental FM<sup>58</sup> and AFM,<sup>59</sup> but not yet for multi-sublattice cases.

Nonetheless,  $S^{(2)}(\mathbf{q}, T)$ , with matrix elements  $M(\epsilon)$  and Fermi factor  $f(\epsilon)$ , is a generalized susceptibility:

$$S^{(2)}(\mathbf{q}; T) \sim \int d\epsilon M(\epsilon) \int d\epsilon' \left[ \frac{f(\epsilon; T) - f(\epsilon'; T)}{\epsilon - \epsilon'} \right] \times \frac{1}{\Omega_{BZ}} \int d\mathbf{k} A(\mathbf{k}; \epsilon) A(\mathbf{k} + \mathbf{q}; \epsilon') \quad (2)$$

$$\rightarrow \int d\mathbf{k} A(\mathbf{k}; E_F) A(\mathbf{k} + \mathbf{q}; E_F). \quad (3)$$

In principle, all states in the valence contribute to (2). If only hole and electron states near  $E_F$  dominate, the bracketed factor [...] yields (3), which is clearly a convolution integral of the Fermi surface states and the origin for “nesting”.<sup>38,56</sup> Due to alloying, even in a metallic system, hybridized states well below  $E_F$  can drive ordering (NiPt<sup>55</sup>) or only features at  $E_F$  (CuPt<sup>57</sup>). For Cr, the NM state yields nesting with an incommensurate wavevector, as observed,<sup>60</sup> while, for Cr-Ru the chemical disorder broadens the FS enough that the SDW now is commensurate, as observed, and coexists with SC.

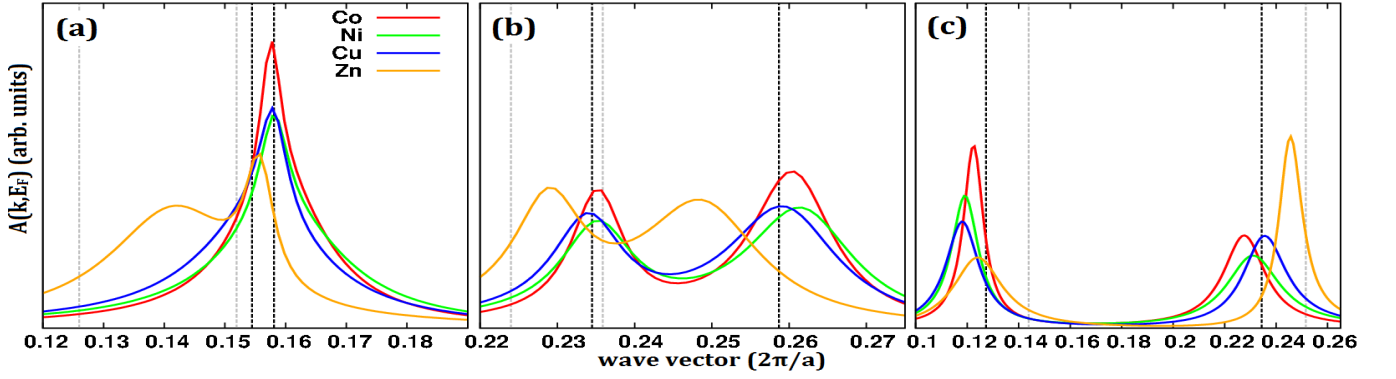


FIG. 3. (Color online) Bloch-spectral function  $A(\mathbf{k}, E)$  along (a)  $X=[1/2, 1/2, 0]$  to  $\Gamma=[000]$ , (b)  $X$  to  $Z=[010]$ , and (c)  $Z$  to  $X$  for Co-, Ni-, Cu-, and Zn-BFA at  $e/\text{Fe} = 0.10$ . These correspond to traversing the principal axes about the hole and electron cylinders. Dark dashed vertical lines correspond to NM rigid-band expectation at same  $e/\text{Fe}$ . The first (second) line is the inner (outer) cylinder. The first (second) light dashed line is for the inner (outer) cylinder of the parent BFA. Notably, in (a), Zn is behaving different than Co, Ni, or Cu, as well as rigid-band.

This discussion was to motivate that the DLM state (with similar FS topology to the NM state) can create similar nesting due to larger volumes of the Brillouin zone contributing to the susceptibility integral, even though the peak overlap is reduced.

### C. Fermi-Surface Nesting in NM State

We analyze the NM Fermi surface (electrons and holes) typically used for SDW stability analysis for a given  $e/\text{Fe}$ . A cross-section of  $A(\mathbf{k}, E_F)$  for transition-metal alloys at fixed  $e/\text{Fe} = 0.10$  are shown in Fig. 3 (in *r.u.*), which traverses from the center of electron (hole) cylinders along principal axes  $k_1 = [110]$  and  $k_2 = [\bar{1}\bar{1}0]$ . Only a range near the spectral peaks is shown in each case. The  $k$ -space broadening is  $\Delta k \sim 0.03$  *r.u.*, much less than the broadening in the DLM case. As can be seen by Fig. 4, it is about the same across dopant species for a given  $e/\text{Fe}$ . The NM rigid-band expectation corresponds to the dark-dashed, vertical lines, while the spectral peaks for the undoped-NM case are marked by grey-dashed line. For Co-, Ni-, Cu-BFA the peaks lie close to the rigid-band expectation both for electron and hole pockets. Only Zn deviates, with peaks in between the old and new levels. This suggests Zn-BFA has a reduced electron doping effect and less interaction with Fe and As bands. Notably, ARPES finds a disagreement between rigid-band lines and the FS of Cu-BFA,<sup>29</sup> and no FS changes for Zn-BFA<sup>24</sup>. However, a DFT study using supercells found a significant shift in the FS of Zn-BFA,<sup>31</sup> but the FS shows considerably more broadening than visible here. Thus, there is an apparent discrepancy in electron itinerancy and effective doping between DFT theory and ARPES experiment.

These effects are alternatively visible in Fig. 4, which shows nested electron and hole cylinders for each doped

compound at  $e/\text{Fe} = 0.10$ . To show the potential nesting overlap, the electron Fermi surfaces have been shifted by wave vector connecting  $X$  and  $\Gamma$  points. On doping the holes shrink and electrons grow. This improved “nesting” (or overlap) leads to a transverse splitting of the nesting vector along  $[1\bar{1}0]$ , as observed for Co- and Ni-BFA.<sup>23</sup> The Zn FS is sharper, indicating longer electron lifetimes. It is visibly shifted from the rigid-band expectation.

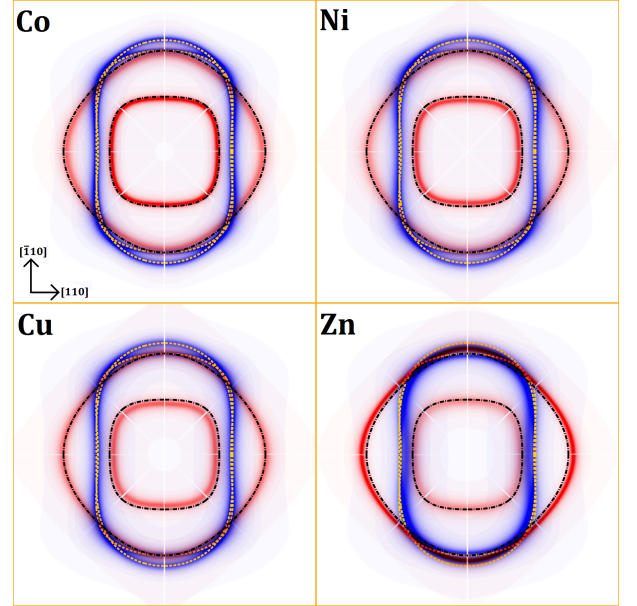


FIG. 4. (Color online) Overlapped electron (blue) and hole (red) pockets of NM doped compounds at  $e/\text{Fe} = 0.10$ . FS for rigid-band shifted NM at the same  $e/\text{Fe}$  are shown as dashed lines (gold) for electron and dash-dot (black) for hole cylinders.



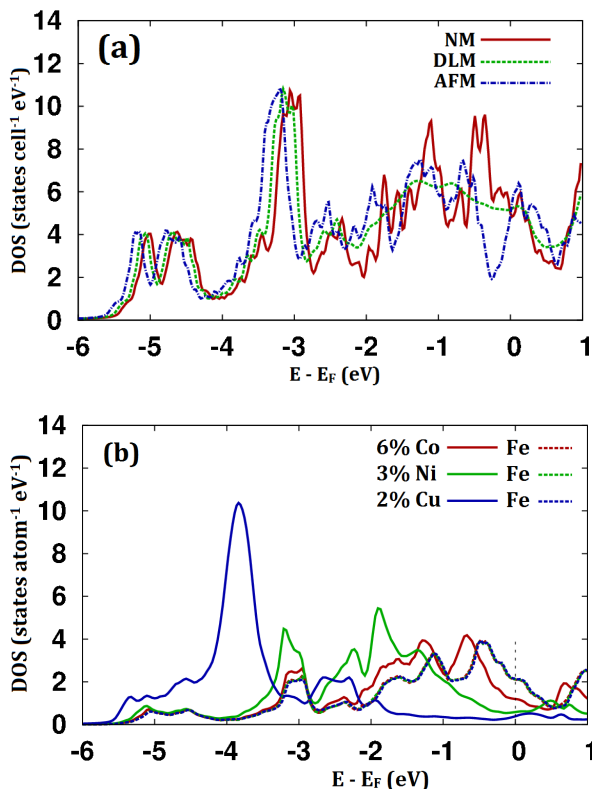


FIG. 5. (Color online) (a) BaFe<sub>2</sub>As<sub>2</sub> DOS relative to E<sub>F</sub> for NM, DLM, and AFM states and (b) Ba(Fe<sub>1-x</sub>M<sub>x</sub>)<sub>2</sub>As<sub>2</sub> dopant site-projected DOS relative to E<sub>F</sub> for 6% Co, 3% Ni, and 2% Cu. Zn states are below -6 eV and show no overlap with the Fe-As valence band. The Fe site projected DOS is the same despite the choice of dopant.

#### D. Density of States and Band Filling

For BaFe<sub>2</sub>As<sub>2</sub> the valence DOS for NM, DLM, and AFM states are shown in Fig. 5, relative to their respective Fermi energies, E<sub>F</sub>. The AFM DOS per primitive (i.e., NM) cell are used to ease comparison. From -6 to -3 eV there is strong overlap of the states, although there is a shift of E<sub>F</sub> due to a pseudo-gap forming below E<sub>F</sub> for AFM state and, more weakly, for the DLM state. This shift is +42 meV (DLM) and +126 meV (AFM) relative to the NM. From -2 to 1 eV the DLM states are significantly broadened due to local spin disorder. Note the average slope for NM and DLM states near the Fermi level is negative. This can explain the apparent Fermi level shift of the DLM visible in Fig. 2. The negative slope and disorder broadening together result in a net reduction in filled states as disorder is turned on. This is compensated by an increased Fermi level. The AFM state shows the opening of a pseudo-gap below the Fermi level, which also explains a large positive shift. The density of states at E<sub>F</sub> (i.e.,  $n(E_F)$ ) are 5.0, 5.2, and 4.8 states-cell<sup>-1</sup>-eV<sup>-1</sup> for NM, DLM, and AFM, respectively.

For Ba(Fe<sub>1-x</sub>M<sub>x</sub>)<sub>2</sub>As<sub>2</sub>, we focus on the valence DOS for NM states versus M in Fig. 5b. The Fe-site projected DOS lie on top of each other for all species M. On the other hand, while significant overlap of Co- and Ni-site projected DOS with Fe-site DOS, there is clearly a split between the Cu-site and Fe-site. These site projections agree with core-electron spectroscopy. The common band behavior of Fe and Co, Ni leads to weak impurity scattering and a limited effect on electronic lifetimes and band structure. Conversely, the split band character of Fe and Cu, Zn leads to strong scattering and a larger influence on total energetics, which includes states well below the Fermi level. This changes the overall energetics and clearly outlines the origin for deviations of Cu, Zn formation energies from Co, Ni in the PM state.

#### V. SUMMARY

In summary, using the all-electron KKR-CPA within DFT, we examined the phase stability, electronic structure, and Fermi-surface evolution of Ba(Fe<sub>1-x</sub>M<sub>x</sub>)<sub>2</sub>As<sub>2</sub> (BFA) with M=Co, Ni, Cu, Zn for nonmagnetic, paramagnetic, and antiferromagnetic states in high-T tetragonal and low-T orthorhombic structures. Hence, both chemical (alloying) and magnetic (orientational) disorder was addressed. Properties were assessed in terms of additional electrons-per-Fe ( $e/\text{Fe}$ ), expected from Hume-Rothery or rigid-band-like behavior. The paramagnetic phase was approximated by a single-site, disordered local moment (DLM) that has a finite, randomly oriented moment on each site (i.e., no magnetic short-range order), which is in contrast to the NM state with zero moments. Magnetic effects are pronounced, leading to significant broadening of the Fermi surface and, so, a reduction in coherent carriers. For the NM state, typically assessed for Fermi-surface nesting instabilities, we find differences versus nominal  $e/\text{Fe}$  in the formation energies, electronic structure, and Fermi-surface properties for Co- and Ni-BFA versus Cu- and Zn-BFA, due to well-known “split-band” behavior. Notably, while Cu-BFA deviates from rigid-band in its formation energetics, it continues to follow the rigid-band expectation in the Fermi-surface evolution; but, Zn-BFA does not follow rigid-band in either formation energetics or Fermi surface behavior. This systematic assessment of the electronic properties for all competing states and structures in BFA should help resolve conflicting interpretations based on different experiments and theories.

#### VI. ACKNOWLEDGEMENTS

Work was supported by the U.S. Department of Energy, Office of Science, Basic Energy Sciences, Materials Science and Engineering Division at Ames (D.D.J.)

and through the Center for Defect Physics (S.N.K.), an Energy Frontier Research Center at ORNL. The Ames

Laboratory is operated for the U.S. DOE by Iowa State University under contract DE-AC02-07CH11358.

- 
- \* snkhan@illinois.edu, ddj@ameslab.gov, aftar@phy.iitb.ac.in
- <sup>1</sup> G. R. Stewart, *Rev. Mod. Phys.* **83**, 1589 (2011).
  - <sup>2</sup> A. A. Kordyuk, *Low Temperature Physics* **38**, 888 (2012).
  - <sup>3</sup> P. M. Aswathy, J. B. Anooja, P. M. Sarun, and U. Syamaprasad, *Superconductor Science and Technology* **23**, 073001 (2010).
  - <sup>4</sup> J. Paglione and R. L. Greene, *Nat Phys* **6**, 645 (2010).
  - <sup>5</sup> H.-H. Wen and S. Li, *Annual Review of Condensed Matter Physics* **2**, 121 (2011).
  - <sup>6</sup> P. C. Canfield and S. L. Bud'ko, *Annual Review of Condensed Matter Physics* **1**, 27 (2010).
  - <sup>7</sup> A. S. Sefat, R. Jin, M. A. McGuire, B. C. Sales, D. J. Singh, and D. Mandrus, *Phys. Rev. Lett.* **101**, 117004 (2008).
  - <sup>8</sup> J.-H. Chu, J. G. Analytis, C. Kucharczyk, and I. R. Fisher, *Phys. Rev. B* **79**, 014506 (2009).
  - <sup>9</sup> N. Ni, A. Thaler, J. Q. Yan, A. Kracher, E. Colambier, S. L. Bud'ko, P. C. Canfield, and S. T. Hannahs, *Phys. Rev. B* **82**, 024519 (2010).
  - <sup>10</sup> N. Ni, M. E. Tillman, J.-Q. Yan, A. Kracher, S. T. Hannahs, S. L. Bud'ko, and P. C. Canfield, *Phys. Rev. B* **78**, 214515 (2008).
  - <sup>11</sup> Y. Nishihara, Y. Yamaguchi, M. Tokumoto, K. Takeda, and K. Fukamichi, *Phys. Rev. B* **34**, 3446 (1986).
  - <sup>12</sup> S. K. Burke and B. D. Rainford, *Journal of Physics F: Metal Physics* **8**, L239 (1978).
  - <sup>13</sup> D. D. Johnson, D. M. Nicholson, F. J. Pinski, B. L. Gyorffy, and G. M. Stocks, *Phys. Rev. Lett.* **56**, 2088 (1986).
  - <sup>14</sup> M. Rotter, M. Tegel, D. Johrendt, I. Schellenberg, W. Hermes, and R. Pöttgen, *Phys. Rev. B* **78**, 020503 (2008).
  - <sup>15</sup> G. Schadler, P. Weinberger, A. Gonis, and J. Klima, *Journal of Physics F: Metal Physics* **15**, 1675 (1985).
  - <sup>16</sup> E. Aktürk and S. Ciraci, *Phys. Rev. B* **79**, 184523 (2009).
  - <sup>17</sup> D. J. Singh, *Phys. Rev. B* **78**, 094511 (2008).
  - <sup>18</sup> J. Fink, S. Thirupathaiah, R. Ovsyannikov, H. A. Dürr, R. Follath, Y. Huang, S. de Jong, M. S. Golden, Y.-Z. Zhang, H. O. Jeschke, R. Valentí, C. Felser, S. Dastjani Farahani, M. Rotter, and D. Johrendt, *Phys. Rev. B* **79**, 155118 (2009).
  - <sup>19</sup> P. Richard, K. Nakayama, T. Sato, M. Neupane, Y.-M. Xu, J. H. Bowen, G. F. Chen, J. L. Luo, N. L. Wang, X. Dai, Z. Fang, H. Ding, and T. Takahashi, *Phys. Rev. Lett.* **104**, 137001 (2010).
  - <sup>20</sup> W. Malaeb, T. Yoshida, A. Fujimori, M. Kubota, K. Ono, K. Kihou, P. M. Shirage, H. Kito, A. Iyo, H. Eisaki, Y. Nakajima, T. Tamegai, and R. Arita, *Journal of the Physical Society of Japan* **78**, 123706 (2009), <http://journals.jps.jp/doi/pdf/10.1143/JPSJ.78.123706>.
  - <sup>21</sup> K. Matan, S. Ibuka, R. Morinaga, S. Chi, J. W. Lynn, A. D. Christianson, M. D. Lumsden, and T. J. Sato, *Phys. Rev. B* **82**, 054515 (2010).
  - <sup>22</sup> T. D. Stanescu, V. Galitski, and S. Das Sarma, *Phys. Rev. B* **78**, 195114 (2008).
  - <sup>23</sup> M. G. Kim, J. Lamsal, T. W. Heitmann, G. S. Tucker, D. K. Pratt, S. N. Khan, Y. B. Lee, A. Alam, A. Thaler, N. Ni, S. Ran, S. L. Bud'ko, K. J. Marty, M. D. Lumsden, P. C. Canfield, B. N. Harmon, D. D. Johnson, A. Kreyssig, R. J. McQueeney, and A. I. Goldman, *Phys. Rev. Lett.* **109**, 167003 (2012).
  - <sup>24</sup> S. Ideta, T. Yoshida, M. Nakajima, W. Malaeb, T. Shimojima, K. Ishizaka, A. Fujimori, H. Kimigashira, K. Ono, K. Kihou, Y. Tomioka, C. H. Lee, A. Iyo, H. Eisaki, T. Ito, and S. Uchida, *Phys. Rev. B* **87**, 201110 (2013).
  - <sup>25</sup> A. S. Sefat, D. J. Singh, R. Jin, M. A. McGuire, B. C. Sales, and D. Mandrus, *Phys. Rev. B* **79**, 024512 (2009).
  - <sup>26</sup> D. J. Singh, *Phys. Rev. B* **79**, 153102 (2009).
  - <sup>27</sup> K. Kudo, M. Takasuga, Y. Okamoto, Z. Hiroi, and M. Nohara, *Phys. Rev. Lett.* **109**, 097002 (2012).
  - <sup>28</sup> Z. Xiao, F.-Y. Ran, H. Hiramatsu, S. Matsuishi, H. Hosono, and T. Kamiya, *Thin Solid Films*, (2013).
  - <sup>29</sup> S. Ideta, T. Yoshida, I. Nishi, A. Fujimori, Y. Kotani, K. Ono, Y. Nakashima, S. Yamaichi, T. Sasagawa, M. Nakajima, K. Kihou, Y. Tomioka, C. H. Lee, A. Iyo, H. Eisaki, T. Ito, S. Uchida, and R. Arita, *Phys. Rev. Lett.* **110**, 107007 (2013).
  - <sup>30</sup> J. M. Luttinger, *Phys. Rev.* **119**, 1153 (1960).
  - <sup>31</sup> T. Berlijn, C.-H. Lin, W. Garber, and W. Ku, *Phys. Rev. Lett.* **108**, 207003 (2012).
  - <sup>32</sup> H. Wadati, I. Elfimov, and G. A. Sawatzky, *Phys. Rev. Lett.* **105**, 157004 (2010).
  - <sup>33</sup> J. Korringa, *Physica* **13**, 392 (1947).
  - <sup>34</sup> W. Kohn and N. Rostoker, *Phys. Rev.* **94**, 1111 (1954).
  - <sup>35</sup> A. Alam, B. Kraczek, and D. D. Johnson, *Phys. Rev. B* **82**, 024435 (2010).
  - <sup>36</sup> B. L. Gyorffy, A. J. Pindor, J. Staunton, G. M. Stocks, and H. Winter, *Journal of Physics F: Metal Physics* **15**, 1337 (1985).
  - <sup>37</sup> D. A. Biava, S. Ghosh, D. D. Johnson, W. A. Shelton, and A. V. Smirnov, *Phys. Rev. B* **72**, 113105 (2005).
  - <sup>38</sup> B. L. Gyorffy and G. M. Stocks, *Phys. Rev. Lett.* **50**, 374 (1983).
  - <sup>39</sup> P. Vilmerscati, A. Fedorov, F. Bondino, F. Offi, G. Panaccione, P. Lacovig, L. Simonelli, M. A. McGuire, A. S. Sefat, D. Mandrus, B. C. Sales, T. Egami, W. Ku, and N. Mannella, *Phys. Rev. B* **85**, 220503 (2012).
  - <sup>40</sup> Z. P. Yin, K. Haule, and G. Kotliar, *Nat Mater* **10**, 932 (2011).
  - <sup>41</sup> V. Crisan, P. Entel, H. Ebert, H. Akai, D. D. Johnson, and J. B. Staunton, *Phys. Rev. B* **66**, 014416 (2002).
  - <sup>42</sup> H. J. Monkhorst and J. D. Pack, *Phys. Rev. B* **13**, 5188 (1976).
  - <sup>43</sup> D. D. Johnson, F. J. Pinski, and G. M. Stocks, *Phys. Rev. B* **30**, 5508 (1984).
  - <sup>44</sup> R. Zeller, *Journal of Physics: Condensed Matter* **16**, 6453 (2004).
  - <sup>45</sup> A. J. Pindor, W. M. Temmerman, B. L. Gyorffy, and G. M. Stocks, *Journal of Physics F: Metal Physics* **10**, 2617 (1980).
  - <sup>46</sup> W. H. Butler and G. M. Stocks, *Phys. Rev. B* **29**, 4217 (1984).
  - <sup>47</sup> L. W. Harriger, H. Q. Luo, M. S. Liu, C. Frost, J. P. Hu, M. R. Norman, and P. Dai, *Phys. Rev. B* **84**, 054544 (2011).

- <sup>48</sup> J. Zhao, D. T. Adroja, D.-X. Yao, R. Bewley, S. Li, X. F. Wang, G. Wu, X. H. Chen, J. Hu, and P. Dai, *Nat Phys* **5**, 555 (2009).
- <sup>49</sup> Q. Huang, Y. Qiu, W. Bao, M. A. Green, J. W. Lynn, Y. C. Gasparovic, T. Wu, G. Wu, and X. H. Chen, *Phys. Rev. Lett.* **101**, 257003 (2008).
- <sup>50</sup> I. I. Mazin and M. D. Johannes, *Nat Phys* **5**, 141 (2009).
- <sup>51</sup> Free energy change per atom is the formation energy plus the ideal mixing entropy, i.e.,  $\Delta s = (2/5)k_B T[x \log(x) + (1-x)\log(1-x)]$ , with annealing  $T=1000^\circ\text{C}$ . The 2/5 arises because Fe/ $M$  occupy only 2/5 of all sites.
- <sup>52</sup> J. Wu, P. Phillips, and A. H. Castro Neto, *Phys. Rev. Lett.* **101**, 126401 (2008).
- <sup>53</sup> W. Setyawan and S. Curtarolo, *Computational Materials Science* **49**, 299 (2010).
- <sup>54</sup> J. B. Staunton, D. D. Johnson, and F. J. Pinski, *Phys. Rev. Lett.* **65**, 1259 (1990).
- <sup>55</sup> F. J. Pinski, B. Ginatempo, D. D. Johnson, J. B. Staunton, G. M. Stocks, and B. L. Gyorffy, *Phys. Rev. Lett.* **66**, 766 (1991).
- <sup>56</sup> J. D. Althoff, D. D. Johnson, and F. J. Pinski, *Phys. Rev. Lett.* **74**, 138 (1995).
- <sup>57</sup> J. F. Clark, F. J. Pinski, D. D. Johnson, P. A. Sterne, J. B. Staunton, and B. Ginatempo, *Phys. Rev. Lett.* **74**, 3225 (1995).
- <sup>58</sup> J. B. Staunton and B. L. Gyorffy, *Phys. Rev. Lett.* **69**, 371 (1992).
- <sup>59</sup> J. B. Staunton, J. Poulter, B. Ginatempo, E. Bruno, and D. D. Johnson, *Phys. Rev. Lett.* **82**, 3340 (1999).
- <sup>60</sup> E. Fawcett, H. L. Alberts, V. Y. Galkin, D. R. Noakes, and J. V. Yakhmi, *Rev. Mod. Phys.* **66**, 25 (1994).